Crystal and Electron Microscopy Structures of Sticholysin II Actinoporin Reveal Insights into the Mechanism of Membrane Pore Formation

José M. Mancheño,[1] Jaime Martín-Benito,[2]
Martín Martínez-Ripoll,[1] José G. Gavilanes,[3]
and Juan A. Hermoso[1,*]
[1]Grupo de Cristalografía Macromolecular
   y Biología Estructural
Instituto Rocasolano
CSIC, Serrano 119
Madrid 28006
[2]Centro Nacional de Biotecnología
CSIC, Campus de la UAM
Madrid 28049
[3]Departamento de Bioquímica y Biología Molecular
Facultad de Química, UCM
Madrid 28040
Spain

Summary

Sticholysin II (StnII) is a pore-forming protein (PFP) produced by the sea anemone *Stichodactyla helianthus*. We found out that StnII exists in a monomeric soluble state but forms tetramers in the presence of a lipidic interface. Both structures have been independently determined at 1.7 Å and 18 Å resolution, respectively, by using X-ray crystallography and electron microscopy of two-dimensional crystals. Besides, the structure of soluble StnII complexed with phosphocholine, determined at 2.4 Å resolution, reveals a phospholipid headgroup binding site, which is located in a region with an unusually high abundance of aromatic residues. Fitting of the atomic model into the electron microscopy density envelope suggests that while the β sandwich structure of the protein remains intact upon oligomerization, the N-terminal region and a flexible and highly basic loop undergo significant conformational changes. These results provide the structural basis for the membrane recognition step of actinoporins and unexpected insights into the oligomerization step.

Introduction

Pore-forming proteins (PFPs) show the remarkable property of existing in at least two definite states. They are synthesized as stable water-soluble monomeric molecules that assemble into oligomeric pores to lyse target cells upon interaction with a membrane. The mechanism of action of PFPs involves protein-membrane interactions, protein-protein interactions, and a special protein-folding pathway underlying the conformational transition from the water-soluble state to the membrane-bound form. PFPs are nowadays considered suitable experimental systems for elucidating the mechanisms of membrane binding, assembly, and insertion (Olson et al., 1999; Heuck et al., 2001). StnII is an actino-

porin (Kem, 1988) produced by the anemone *Stichodactyla helianthus* (order Actiniaria), currently classified as a transmembrane solute transporter from the pore-forming equinatoxin family 1.C.38 (Saier, 2000). Actinoporins are PFPs displaying similar molecular masses (∼20 kDa) and high isoelectric points (pI's > 9.0), related to each other in amino acid sequence (∼66%–85% identity), and presumably sharing a common mechanism of pore formation (Anderluh and Macek, 2000).

Actinoporins are cytotoxic and lytic toward a variety of cells and organelles. In fact, StnII was initially described as a potent hemolytic agent which increased membrane permeability to small ions and solutes through pore formation (Berheimer and Avigad, 1976; Michaels, 1979; Varanda and Finkelstein, 1980). Numerous studies on the effects of actinoporins on model membranes support a mechanism of bilayer permeabilization through oligomeric pores (De los Ríos et al., 1998; Valcárcel, et al., 2001). Although sphingomyelin-containing membranes are especially susceptible to actinoporins, other lipid systems are also permeabilized (De los Ríos et al., 1998). The widespread cytotoxicity of actinoporins (Macek et al., 1995) would be related to the ubiquitous presence of sphingomyelin, a low-affinity acceptor, in animal cells.

In contrast to bacterial PFPs (Macek et al., 1995; Song et al., 1996; Stroud et al., 1998; Billington et al., 2000), the mechanism of actinoporin pore formation is poorly defined, due in part to the scarcity of structural information (Martín-Benito et al., 2000; Athanasiadis et al., 2001; Hinds et al., 2002). To elucidate the structural basis of pore formation of the actinoporin family, we have determined the three-dimensional structures of the monomeric water-soluble state of StnII and that of the complex StnII:phosphocholine (POC) at 1.7 and 2.4 Å resolution, respectively, and also carried out electron crystallographic analysis of two-dimensional crystals of the toxin on a lipidic interface. The combination of the low-resolution electron microscopy (EM) maps with atomic structures is nowadays a powerful tool to determine conformational changes in large protein assemblies (Saibil, 2000). In our case, this approach revealed that upon interaction with a lipidic interface, a tetrameric oligomer is formed in which the individual StnII protomers would maintain intact their β sandwich core but would undergo conformational changes in the N-terminal region and in a highly basic and flexible loop, near the POC binding site.

Results and Discussion

Description of the Water-Soluble Form of StnII Structure

The water soluble monomer of StnII has a globular shape with dimensions of 45 × 32 × 27 Å. The resulting structure is based on a β sandwich fold composed of ten β strands, flanked on each side by two short α helices (Figure 1). The two β sheets of the sandwich structure

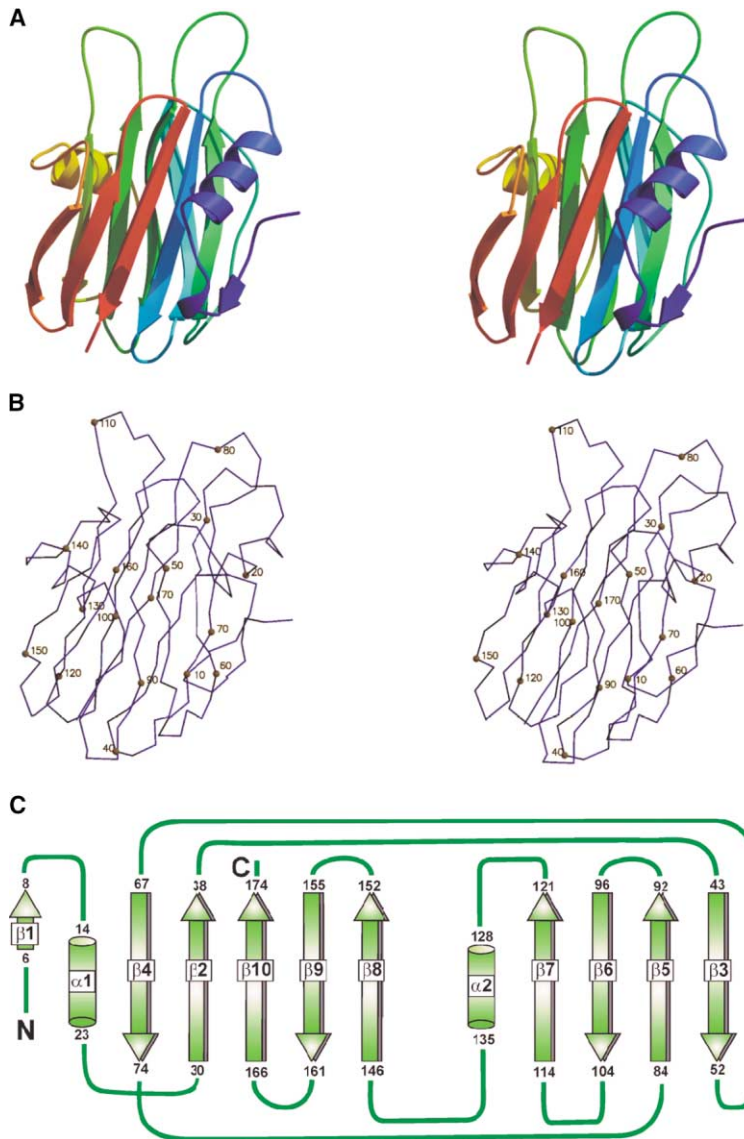*Correspondence: xjuan@iqfr.csic.es

Figure 1. Overall Structure of StnII

(A) Stereo view ribbon diagram of Stn II. The sequence is shaded from blue at residue 1 to red at residue 175.

(B) Stereo α-carbon trace, same view as for (A), with balls and numbers marking every 10 residues.

(C) Topology diagram of StnII. α helices and β strands are represented by cylinders and arrows, respectively. The α helix and β strand identifiers are α1 and α2, and β1 to β10, respectively. The residue range for every secondary structure element is also given. (A) and (B) were prepared with Bobscript (Esnouf, 1997) and subsequently rendered with Raster3D (Merritt and Murphy, 1994).

consist of the five and four strands, respectively (Figure 1C). The helices α1 and α2 are located between the strands β1 and β2, and β7 and β8, respectively. They predominantly interact with the β sandwich through hydrophobic interactions and ten and seven van der Waals contacts, respectively, although salt bridges are also observed (Asp 18-Lys 168 and Asp 133-Lys 118).

The analysis of the Stn II structure revealed the striking presence of an exposed cluster of aromatic amino acids composed of Tyr106, Trp110, Tyr111, and Trp114 (coming from the loop comprised between strands β6 and β7), and Tyr131, Tyr135, and Tyr136 from helix α2. These residues are known to have affinity for the membrane interface (Killian and von Heijne, 2000), and in fact, analogous clusters have been observed in bacterial channel-forming toxins such as α-hemolysin (Song et al., 1996) and aerolysin (Parker et al., 1994). In this regard, recent biochemical studies on the actinoporin equinatoxin II (EqtII) have shown the participation of the equivalent region in membrane binding (Hong et al., 2002). Remark-

ably, the segment comprising residues 108–111 of StnII is the only region of the structure that could not be placed in the electron density, suggesting that this loop is highly mobile. A high degree of conformational flexibility in this region, which is essential for binding of POC (see below), may allow an efficient adaptation of StnII to the membrane surface. In this sense, POC binding stabilizes this loop, as deduced from the comparison of the corresponding electron density maps.

Three-dimensional structural alignment using Dali (http://www2.ebi.ac.uk/dali/) showed that StnII is structurally similar to several other β sandwich-containing proteins, presumably because of the widespread distribution of this structural motif in functionally diverse proteins. As expected, StnII is most similar to EqtII (PDB entry 1IAZ; 172 Cα atoms superpose with an rms deviation of 0.6 Å). Comparison of both structures (Figure 2) revealed that while the β sandwich core is essentially conserved, significant main chain deviations are observed in important functional loops, mainly the loop
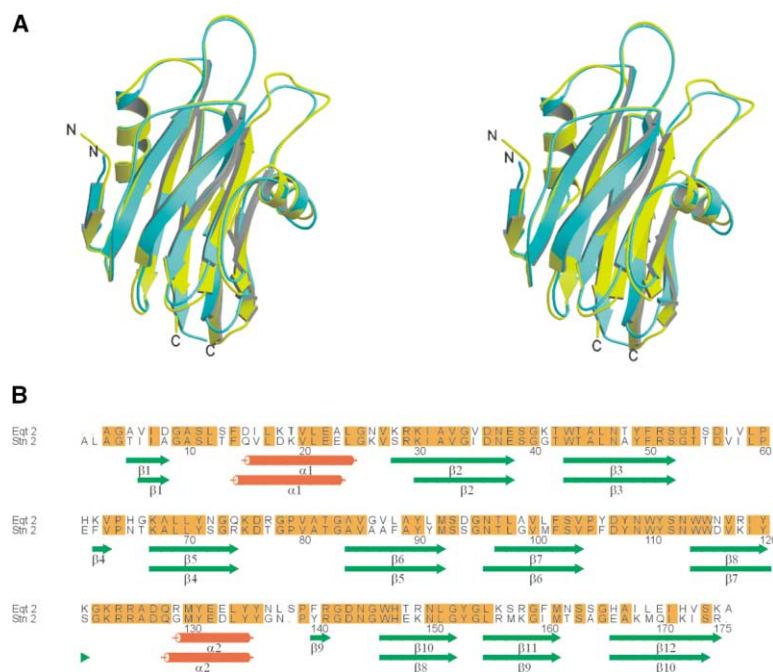
A

B

Figure 2. Structural Comparison between StnII and EqtII

(A) Stereo view showing the three-dimensional superposition of StnII (yellow) and EqtII (cyan).

(B) Sequence alignment of StnII and EqtII. Residues highlighted in orange are identical. The secondary structure elements of both proteins are shown as green arrows (β strands) and red cylindres (α helices). Numbering refers to the sequence of StnII. Sequence alignment was generated with the program Clustalx (Thomson et al., 1997), and the figure was prepared with Alscript (Barton, 1993).

between strands β6 and β7 in StnII (see below). Weaker similarities were also detected, the most significant being thaumatin (PDB entry 1THV), the tick-borne encephalitis virus glycoprotein (PDB entry 1SVB), and the α subunit of the clathrin adaptor ap-2 (PDB entry 1QTS-A), with rms deviations of 2.8, 3.4, and 3.7 Å for 96, 86, and 85 Cα atoms, respectively. A significant similarity was also found with the β sandwich domain 4 of perfringolysin O from *Clostridium perfringens* (76 Cα atoms superpose with an rms deviation of 2.8 Å), the other pore-forming toxin that scored over the default significance level.

The Phosphocholine Binding Site

A fundamental issue associated with the mechanism of membrane interaction of any PFP is the identification and structure resolution of the protein domain involved in lipid recognition (Heuck et al., 2001). Cocrystals of StnII with POC revealed for the first time the existence of a POC binding site in a member of the actinoporins family (Figure 3A). Biochemical evidences revealing POC binding by StnII in solution come from the inhibitory effect exerted by this molecule on the kinetics of liposome permeabilization promoted by StnII (data not shown). Phosphocholine binds to a cavity with overall dimensions of $9 \times 11 \times 13$ Å. This cavity is partly hydrophilic due to the phenolic hydroxyl groups of Tyr131, Tyr135, and Tyr136 and the side chains of Ser52 and Ser103, and partly hydrophobic because it contains the side chains of Val85 and Pro105 and the aromatic rings of Tyr111 and Tyr135. Remarkably, all residues conforming the POC binding site are strictly conserved in the 3D structure of EqtII, the only actinoporin with 3D structure so far described (Athanasiadis et al., 2001; Hinds et al., 2002).

The positive charge of choline moiety is stabilized by cation-π interactions between the electron-rich systems of the aromatic rings of Tyr111 and Tyr135. Besides, the phosphate moiety interacts with the phenolic hydroxyl groups of Tyr111 and Tyr136 and presumably would be further stabilized by the cationic side chain of Arg51 (Figure 3A). Interestingly, comparison of the structures of free StnII and that of the complex StnII:POC revealed some backbone modifications in the loop between strands β6 and β7 (rmsd 0.71 Å versus an overall value of 0.30 Å). However, the structural differences are mostly due to side chain rearrangements to facilitate POC binding (Figure 3B). Cation-π interactions (Gallivan and Dougherty, 1999) between aromatic residues and POC have been also observed in the crystal structure of Staphylococcal LukF complexed with POC (Song et al., 1996; Olson et al., 1999) and, most recently, in the substrate binding pocket of human phosphatidylcholine transfer protein (Roderick et al., 2002) and in other alkylamine binding proteins (Bellamy et al., 1989; Sussman et al., 1991).

3D Electron Microscopy Structure of StnII on Lipid Monolayers

Two-dimensional crystals of StnII were grown on lipid monolayers as described in the Experimental Procedures section. The samples yielded ordered areas in around 15%–20% of the monolayers, which showed a substantial degree of bending due to the flexibility of the monolayers. As a result of that, high-quality crystalline patches were small, thus making unfeasible the use of cryoelectron microscopy. Six micrographs of negatively stained crystals as that shown in Figure 4A, all of them reaching 15 Å resolution, were merged to generate a projection map without any symmetry imposition (Figure 4B). The 2D crystals belong to the $P42_12$ space group, with unit cell dimensions of 163×163 Å. Each cell contained eight molecules of StnII arranged in two tetrameric assemblies. Imposition of the $P42_12$ symmetry
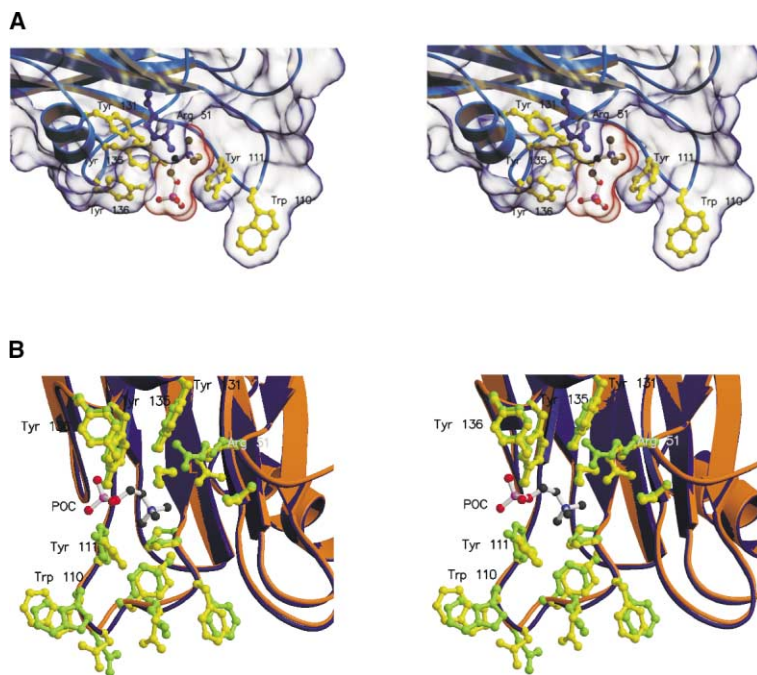
A

B

Figure 3. Phosphocholine Binding Site of StnII and Amino Acid Residue Rearrangements upon POC Binding

(A) GRASP (Nicholls et al., 1991) molecular surfaces of StnII (blue) and of the bound phosphocholine (red). Some residues thought to be important for phosphocholine binding are shown.

(B) Stereo view of the superposition of free StnII (orange) and the StnII:POC complex (dark blue), showing residue rearrangements (green for free StnII and yellow for StnII:POC complex) in the POC binding site. This figure was prepared with Bobscript (Esnouf, 1997) and subsequently rendered with Raster3D (Merritt and Murphy, 1994).

(Figure 4C) did not introduce any major change in the structural features of the projection map generated with *P*1 symmetry, which reveals the quality of the data. The presence of three mutually perpendicular symmetry axes reveals a high level of symmetry within the 2D crystal. Whereas both 2-fold axes are located in the plane of the monolayer, the 4-fold symmetry axis is perpendicular to the lipid interface and relates the four StnII molecules that form the tetramers. Interestingly, the 2-fold screw axis passes through the center of the oligomer, which originates an up-and-down pattern of identical tetramers with respect to the lipid monolayer.

Out of 204 micrographs, 52 images with tilt angles ranging from −52° to 57° were selected, processed, and combined in the P4$_2$1$_2$ space group to generate a 3D map of the structure of StnII in the lipid interface. The final 3D map was filtered at 18 Å resolution. As suggested by the 2D projection maps, the 3D reconstruction of StnII in the lipid monolayer showed tetrameric assemblies that defined an inner pore (Figures 5 and 6). In this regard, it is interesting to note that recent biochemical evidences obtained from chemical crosslinking and analytical ultracentrifugation studies showed that StnII is an associating protein (De los Ríos et al., 1999a). Each equivalent monomer within the assembly exhibits a curved and thin shape in contrast to the globular, soluble structure of monomeric StnII. This result agrees with previous structural analyses on the EM structure of StnII (Martín-Benito et al., 2000). The 2D crystals analyzed in this last study did not reveal the existence of continuous oligomeric assemblies; only monomeric forms with an essentially identical structure as that of one protomer of the tetrameric assembly herein reported were observed. All these facts are consistent with the hypothesis proposed for EqtII in which the N-terminal region changes its conformation after membrane binding while in the monomeric state (Hong et al., 2002; Malovrh et al., 2003).

The tetrameric assembly showed distinct wide and narrow regions. The maximum outer diameter in the narrow region is 95 Å, and 110 Å in the wide one, and their pores have an inner diameter of 50 Å, with a height of 43 Å. The M$_r$ of the tetramer calculated from the 3D map is ∼76 kDa, assuming an average protein density of 0.75 Da Å^{-3} (the M$_r$ of the StnII monomer is 19.25 kDa), which strongly suggests that StnII does not significantly insert into the lipid monolayer.

Conformational Changes of StnII upon Oligomerization at the Lipid Interface

A high-resolution model of the StnII tetramer was constructed by docking the atomic model of the soluble StnII into the 3D reconstruction (Figures 6A and 6B). This was facilitated by the excellent fit of the β sandwich into the EM envelope and by the existence of a bulge in the 3D map, since the unique protruding structural elements of StnII are the loops between strands β4 and β5, and β6 and β7. Fitting the first loop into the bulge rendered a conceivable model of the StnII tetramer (Figure 6A). This model predicts that the β sandwich core of the StnII structure would not suffer significant conformational changes upon oligomerization, as deduced by its perfect fitting into the EM map. Moreover, the only regions clearly out of the density envelope, and thus presumably involved in conformational changes, are the N-terminal region (from Ala1 to Val27), the highly basic loop between strand β7 and helix α2 (121Ser-Gly-Lys-Arg-Arg-Ala-Asp-Gln128), and part of this helix (from Gly129 to Asp133). Furthermore, this model suggests that a simple pseudorigid body movement of the N-terminal region about the loop between helix α1 and strand β2, particularly a rotation between Ser28 and Arg29, would be sufficient to fill up the EM density in between monomers (Figure 6C). Consequently, the N-terminal region would be initially involved in oligomerization through
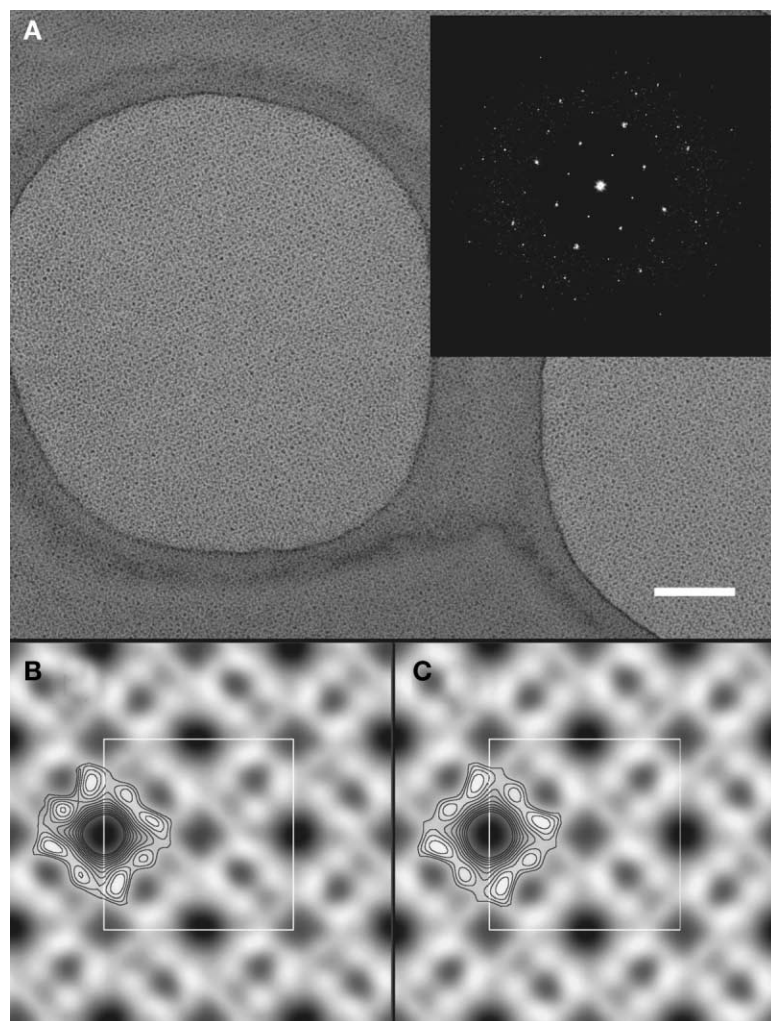
Figure 4. Two-Dimensional Crystals of StnII on Lipid Monolayers

(A) TEM micrograph of a negatively stained 2D crystal of StnII. Pore-shaped structures are clearly observable arranged in a squared array. The inset shows the computed diffraction pattern. Note the characteristic systematic absences in the (2h+1,0) and (0, 2k+1) reflections, consistent with the symmetry group P42$_1$2. Scale bar: 100 nm.
(B) Projection map without any symmetry imposition.
(C) Projection map with P42$_1$2 symmetry. The unit cell is indicated as a white box that contains eight molecules of protein. In both cases the same tetrameric structure has been contoured attending to levels of gray in order to show that the symmetry imposition does not introduce any major changes in the features of the projection map.

interactions with the C-terminal region of the adjacent monomer. Thus, the loop between helix α1 and strand β2 would be essential for this conformational change, acting as a hinge segment.

The existence of an in-plane 2-fold screw axis passing through the center of the tetramers in the StnII 2D crystal suggests that the POC binding site does not provide StnII the required driving force for binding to this phosphatidylcholine monolayer; presumably, other structural details of the target membrane must be recognized for membrane binding to occur. Nevertheless, one of the tetramer orientations observed in the 2D crystal is highly inspiring, because according to the above high-resolution model of the tetramer: (1) the orientation of the POC binding site is the expected for the membrane interface, (2) there are many additional aromatic residues that would face the membrane (Trp110, Trp114, Tyr140, Tyr153), (3) the other loops interacting with the lipid headgroup region, the ones between strands β5 and β6 (93Ser-Ser-Gly-Asn96), and β8 and β9 (152Gly-Tyr-Gly-Leu155) show an amino acid composition energetically compatible with its transfer from water to a lipid interface (Wimley and White, 1996), and (4) the basic loop between strand β7 and helix α2 is located near the lipidic inter-face, which would permit its interaction with the phosphate region of the lipids, thus further anchoring the protein to a target membrane. In addition, this model revealed a satisfactory correlation between the functional regions of StnII (those that would interact with the lipidic interface together with the hinge segment and the basic loop) and the distribution of the Cα-atom B factor values, since these regions are the most flexible parts of the StnII molecule according to their B factor values (Figure 6B).

A Putative Model for the Mechanism of Actinoporin Pore Formation

The process of actinoporin membrane binding proceeds through a sequential mechanism involving at least two discrete steps, as shown recently (Hong et al., 2002). After initial binding of the monomer to the membrane surface, a subsequent step involves a conformational change in the N-terminal region of the protein that has been proposed to traverse the bilayer, thus forming the transmembrane pore. The results we herein presented provide unexpected structural insights into the mechanism of actinoporin pore formation.

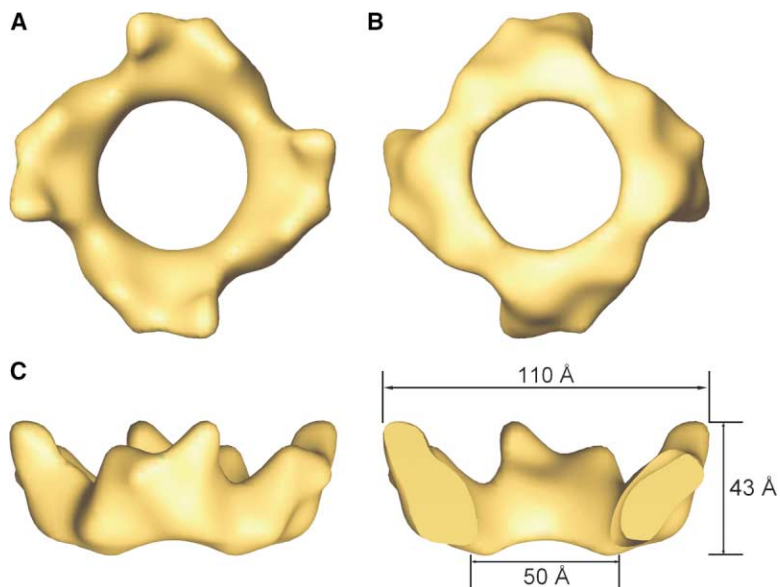3D crystallization of the soluble StnII has yielded both

Figure 5. The Three-Dimensional Reconstruction of the StnII Tetrameric Assembly on a Lipid Monolayer

Top (A), bottom (B), and side and cut open (C) views of the oligomer. The final structure was calculated from 204 micrographs combined in the P42₁2 space group (details in the text).

the high-resolution structure of the native StnII and that of the complex StnII:POC. Sequence comparison among the actinoporins and structural analysis with the 3D structure of EqtII (Figure 2) suggest that the POC binding site is a common structural motif for all of them. The analysis of this domain offers new insights into the molecular basis of the specific lipid recognition of sphingomyelin (SM) by actinoporins. Although other structural details than the lipid headgroup must be recognized by the toxin for membrane binding to occur, the existence of a POC binding site together with additional exposed aromatic residues would provide these PFP's with an important driving force for the initial attachment of the toxin to the membrane interface. In this sense, previous results obtained with EqtII agree with the existence of such a binding domain. Thus, the *critical* roles of Trp112 and Trp116 of EqtII (Trp110 and Trp114 in StnII) in membrane binding (Hong et al., 2002) can be easily rationalized in terms of a specific POC binding site. Furthermore, all single cysteine mutants of EqtII affecting this domain directly (Ser54, Ser105) or indirectly (Ser114, Glu134) showed very reduced hemolytic (except Ser105 mutant) or permeabilizing activities (Anderluh et al., 1999). Also, Ser105 and Ser114 of EtqII (Ser103 and Ser112 in StnII) were proposed to have an interfacial location, which is in excellent agreement with our model.

2D crystallization of StnII on lipid monolayers has revealed for the first time the presence of stable tetrameric pore-shaped structures endowed with 4-fold symmetry (Figure 5). Since oligomeric structures of StnII are not observed in the protein packing of 3D crystals, it can be deduced that the information necessary for StnII oligomerization is contained within the system composed of toxin *and* the water/lipid interface, i.e., oligomerization is not exclusively driven by a protein concentrating effect.

Docking of the atomic model of StnII into the 3D reconstruction rendered a plausible high-resolution model of the StnII tetramer formed upon oligomerization that predicts: (1) the preservation of the β sandwich structure, (2) the existence of conformational changes of the protein affecting the N-terminal region and the highly basic loop between strand β7 and helix α2, (3) the regions involved in oligomerization (the N-terminal segment, the loop between strands β2 and β3 and the C-terminal end), and (4) the regions that would directly interact with the membrane interface (the POC binding site and the loops between strands β5 and β6 and β8 and β9). Previous experimental results reinforce the validity of this model. Thus, it has been shown that the N-terminal helix of EqtII must translocate from the β sandwich to the membrane to form a functional pore (Hong et al., 2002). According to our model, the N-terminal region changes its conformation upon oligomerization; this conformational change can be easily explained by a simple pseudorigid body movement of the N-terminal segment about the above mentioned hinge segment. Interestingly, mutants of EqtII affecting this loop either directly (Arg31; Arg29 in StnII) or indirectly by mutating nearby residues (Lys77; Lys75 in StnII) have been shown to exhibit drastically reduced hemolytic and permeabilizing activities (Anderluh et al., 1999). Furthermore, the existence has been shown of rearrangements around residues Lys43 and Ser95 of EqtII (Gly41 and Ser93 in StnII) upon membrane interaction (Anderluh et al., 2000), which according to our model would be situated in a region directly contacting the N-terminal segment of the adjacent monomer (Gly41), and in a loop predicted to directly interact with the membrane (Ser93).

Considering the above results, a model for the mechanism of actinoporin pore formation can be envisaged. The mechanism would proceed through at least three steps: monomer binding to the membrane interface, assembly of four monomers, and final formation of the functional pore. Binding of soluble monomers to the membrane surface would be mainly driven by the affinity they exhibit for the phosphocholine group of lipids (POC binding site) and also for the water/lipid interface (additional exposed aromatic residues), although other structural details of the lipids must be recognized for effective
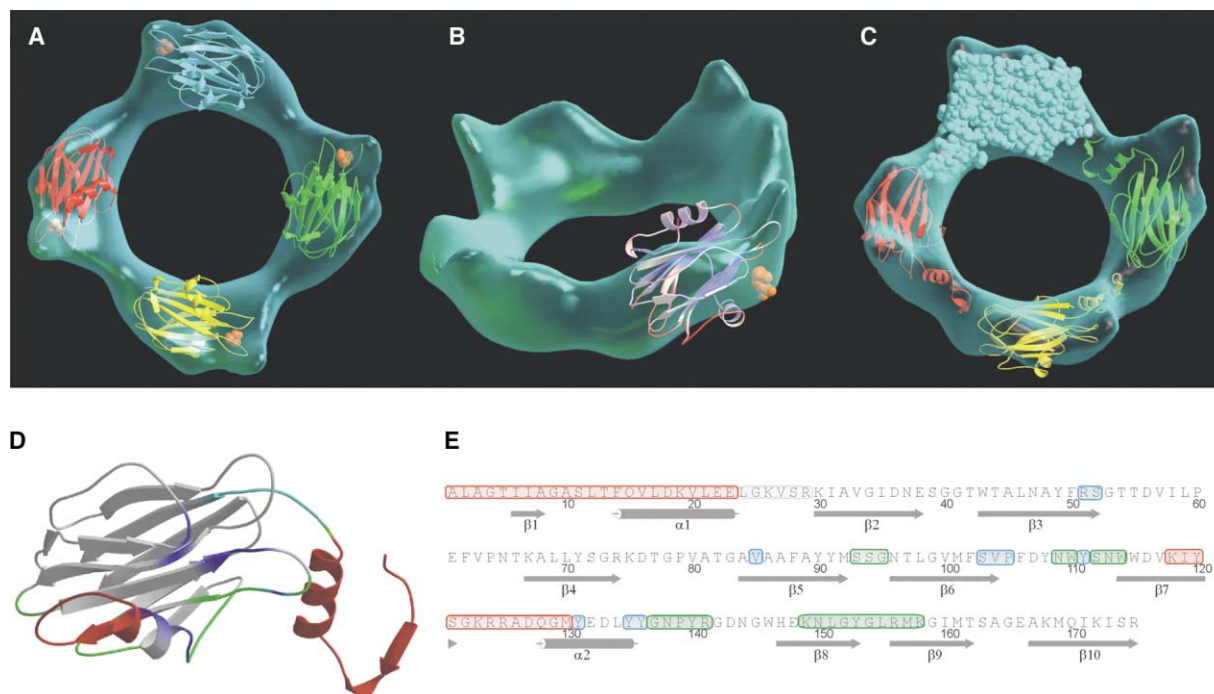
Figure 6. Model of the Sticholysin II Tetramer and Functionally Important Regions of StnII

(A) Top view of the fit of the high-resolution structure of monomeric water-soluble StnII into the EM density. Each subunit is indicated by a different color. Note that the N-terminal region and the loop before helix α2 clearly protrude from the EM density.

(B) Tilted view of the tetramer in which a unique X-ray monomer has been colored according to the Cα B factor values (color ramping from blue to red, from low to high B factor values). Phosphocholine molecules are shown as orange cpk models.

(C) Putative model exhibiting conformational changes in StnII upon tetramer formation. View of the fit of the modified StnII water-soluble atomic model into the EM density. The N-terminal segment has been moved by rotation about the loop following helix α1. A monomer is highlighted as a cyan cpk model.

(D) Ribbon diagram of one protomer of StnII in which functionally relevant regions are given in different colors: red, regions suffering conformational changes upon oligomerization in the lipid interface; cyan, hinge segment for N-terminal region movement; blue, POC binding site; green, membrane-interacting segments different from the POC binding site.

(E) StnII sequence with the proposed functional regions highlighted as in panel (D). Panels (A), (B), (C), and (D) were prepared with Bobscript (Esnouf, 1997) and subsequently rendered with Raster3D (Merritt and Murphy, 1994). Panel (E) was prepared with Alscript (Barton, 1993).

binding. After adsorption to the membrane surface, four protein molecules would associate, forming an oligomeric assembly similar to that found in the 2D crystals. This step would involve changes in the conformation of the protein molecules mainly affecting both the N-terminal segment (Ala1 to Arg29) and a flexible and basic loop (Ser121 to Gln128). While the first segment would be initially involved in protein-protein contacts, the second would further anchor the protein to the membrane (Figures 6 and 7). Regarding to the final step of the mechanism, i.e., formation of the functional pore, it has been recently proposed that StnII originates toroidal pores in the membrane (Valcárcel et al., 2001), similar to those formed by other toxic peptides (Yang et al., 2002), particularly melittin, which shows structural homology with the N-terminal end of actinoporins (Belmonte et al., 1994). According to this, both protein molecules and lipids would form the walls of the pore. Considering the high-resolution model of the tetrameric assembly, a tentative hypothesis for this last step can then be proposed which would involve the extension of the N-terminal region of each protomer, which would adopt a helical conformation (Figure 7). In this regard, very recently it has been proposed that the N-terminal segment of EqtII (from

Asp10 to Asn28) adopts an α-helical conformation in the functional pore that forms a tilting angle of around 21° with respect to the plane of the membrane (Malovrh et al., 2003), which agrees well with our proposed model (tilting angle ∼30°). These helical segments together with lipid molecules would line the pore which has a diameter <3 nm, close to the diameter of the functional pore (De los Ríos et al., 1998; Valcárcel et al., 2001) (diameter ∼2 nm). Additionally, this model agrees well with the fact that recombinant StnII with a $(His)_6$-tail in the N-terminal end permeabilizes membranes as the natural StnII (De los Ríos et al., 1999b), and also with truncation experiments of the N-terminal end with EqtII (Anderluh et al., 1997). Moreover, this model predicts the existence of potential intermonomer interactions, particularly, the presence of a network of ionic interactions between the positively charged C-terminal residue Arg175 and Glu23 of the adjacent monomer.

In conclusion, the finding of a POC binding site in a member of the actinoporins family offers unexpected insights into the structural basis for actinoporin lipid recognition. In addition, the high-resolution model of the StnII tetramer is consistent with experimental studies providing the structural basis for previous functional

A

B
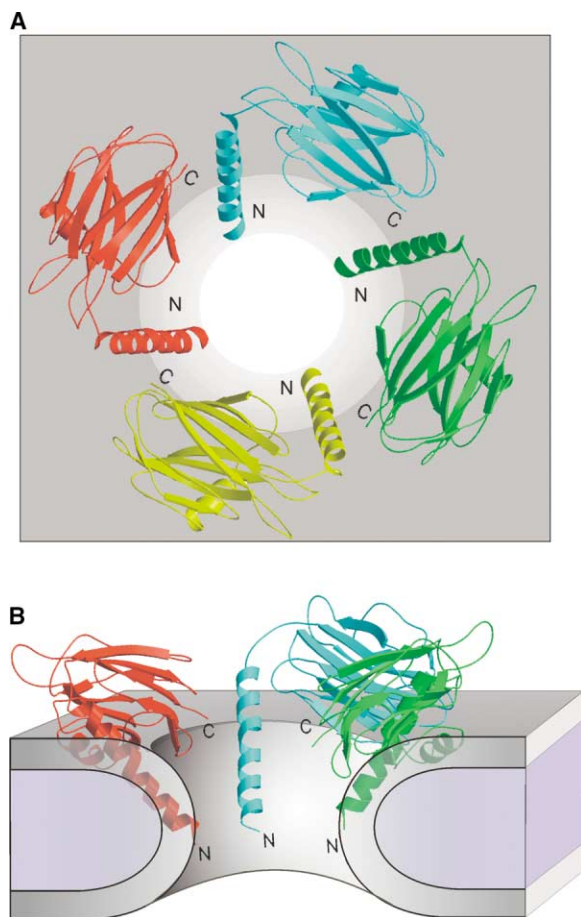
Figure 7. Tentative Model of the Functional Pore of StnII

(A) Top view of the putative functional StnII pore, in which four StnII monomers are shown in different colors.

(B) Front view of the same pore, with the yellow monomer omitted for clarity. The lipid headgroup regions are indicated as gray layers. Note that the walls of the pore would be lined by four helices and lipid molecules.

hypotheses and also predicting new functional regions, i.e., a hinge segment and the basic loop. Future studies will concentrate on the structural basis of the last step of the mechanism of pore formation, taking into account the above model as working hypothesis.

Experimental Procedures

2D and 3D Crystallization

StnII purified as previously described (De los Ríos et al., 1998) was dissolved in 20 mM Tris buffer (pH 7.0) at 6–8 mg/ml. The mother liquor used for hanging drop vapor diffusion crystallization consisted of 0.2 M lithium sulfate, 0.1 M Tris buffer (pH 7.5), and 25%–30% (w/v) PEG 4000. Crystals of the StnII-phosphocholine complex were obtained by soaking preformed StnII type I crystals in a solution containing mother liquor plus 20 mM POC for approximately 20 s. After soaking, the crystals were immediately flash-cooled under a nitrogen stream.

Two-dimensional crystals of StnII on lipid monolayers were prepared essentially as described (Martín-Benito et al., 2000) with several modifications. The synthetic phospholipid 1,2-dioleoyl-sn-glycerol-3-phosphorylcholine (DOPC) was used instead of PC (phosphatidylcholine) from egg yolk. Additionally, the crystallization time was increased to ∼12 hr. This new experimental procedure

Table 1. Structure Determination and Statistics for Native StnII (Type I and II Crystals), StnII:Phosphocholine Complex, and Electron Crystallographic Data

	StnII(I)	StnII(II)	StnII:POC
Space group	P2₁	P2₁	P2₁
a (Å)	32.30	32.86	32.63
b (Å)	119.73	43.57	43.25
c (Å)	43.42	120.03	119.52
β (°)	90.04	92.43	92.73
Data collection			
Wavelength (Å)	1.004	1.542	1.542
Resolution (Å)	32.3–1.7	29.5–2.2	29.9–2.4
Unique reflections	31889	15860	12965
Redundancy	2.1	4.0	4.6
Completeness (%)	90.3	98.1	98.7
I/σ(I)	5.0	5.1	7.2
R$_{merge}$	8.6	11.0	9.2
Refinement statistics			
Protein nonhydrogen atoms	2722	2722	2722
Ligand nonhydrogen atoms	40	36	22
Solvent nonhydrogen atoms	373	142	145
Resolution range (Å)	10.0–1.7	10.0–2.2	15.0–2.4
R$_{work}$ (%)	21.6	21.5	21.2
R$_{free}$[a] (%)	25.6	26.9	26.9
Rmsd bonds (Å)	0.005	0.007	0.007
Rmsd angles (°)	1.30	1.30	1.40
Average B factor (Å²)	18.4	29.4	26.5
Electron crystallographic data			
Space group	P42₁2		
a (Å)	163		
b (Å)	163		
Number of images	52		
Unique reflections	2775		
Overall weighted phase residual (°)	26.8		

[a] R calculated for 5% of data excluded from the refinement.

provided repetitive high-quality 2D crystals in terms of resolution and size of crystal areas.

Structure Determination

Data were collected at the ESRF (Grenoble, France) on frozen type I crystals of StnII (beamline BM14, wavelength 1.004 Å), and in-house on a MAR Research MAR345 imaging-plate detector with Cu Kα rays generated by an Enraf-Nonius rotating-anode generator on frozen type II crystals of native StnII or cocrystals of StnII and POC. All data were processed with MOSFLM (Leslie, 1994) and SCALA (CCP4, 1994) (Table 1). Type I StnII crystals belong to the monoclinic P2₁ space group and have unit cell parameters of a = 32.3 Å, b = 119.7 Å, c = 43.4 Å, β = 90.0°. Type II StnII crystals or StnII-POC cocrystals were also monoclinic (P2₁ space group) and have cell parameters of a = 32.6 Å, b = 43.2 Å, c = 119.5 Å, β = 90.7°.

Initial phases for the StnII measured intensities (type I crystals) were obtained by molecular replacement with the program MolRep (CCP4, 1994) using the structure of EqtII (PDB accession code 1IAZ) (Athanasiadis et al., 2001) as starting model. Initial phases for StnII (type II crystals) and the StnII-POC complex were obtained using the refined StnII coordinates with AmoRe (Navaza, 1994).

Model Building and Refinement

The first molecular model for StnII was built to 1.7 Å with O (Jones et al., 1991), and refinement was carried out with REFMAC (CCP4, 1994). The second molecular model for StnII and the complex StnII-POC, both from type II crystals, were built to 2.2 Å and 2.4 Å with O (Jones et al., 1991) using the first refined StnII structure as starting model. Refinement was carried out with CNS (Brünger et al., 1998) with the maximum likelihood function target. Simulated annealing

was used in the initial steps, and cycles of conventional positional refinement and restraint individual B factor refinement were used in the last stages. Refinement statistics are given in Table 1. The conformation of StnII in type I and II crystal forms is almost identical (the root mean square [rms] deviation in main chain atomic positions is 0.22 Å); the only significant differences being localized at residues Lys26, Gly78, Asp107, and Asn109, all of them located in solvent-exposed loops.

Electron Microscopy and Image Processing
Two-dimensional crystals of StnII were examined in a JEOL 1200 EXII (JEOL Co.) transmission electron microscope operated at 100 kV. Micrographs were taken under low dose conditions at a calibrated magnification of 39,000× and a nominal underfocus of 2,000–7,000 Å. The image quality and the crystalline order of the crystals were evaluated by using the CRISP software (Hovmöller, 1992). The best micrographs were digitized with Zeiss PhotoScan TD (Z/I Imaging) at a sampling resolution of 3.6 Å/pixel and processed with the MRC image processing programs (Crowther et al., 1996). This process includes the correction of distortions by correlation and averaging methods (Henderson et al., 1986) and CTF detection using ICE software (Hardt et al., 1996). The crystallographic space group was determined using the program ALLSPACE (Valpuesta et al., 1994).

Three-Dimensional Reconstruction
A total of 52 images with tilt angles ranging from −52° to 57° were used. Six untilted images were merged using the program ORIGTILT from the MRC software (Crowther et al., 1996) and symmetrized to be used as a reference set. Tilted images were subsequently merged in ascending order attending to tilt angle and following the ideas developed by Amos et al. (1982). The real tilt was calculated using the formulas of Shaw and Hill (1981). The average resolution was 15 Å for images between 0° to 20°, 17 Å for images between 20° and 40° tilt, and 20 Å for images between 40° and 57° tilt. Merging was performed using the space group P42$_1$2, and the phase origin refinement was carried out using reflections with quality index better than 6 (2775 unique reflections) (Table 1). The lattice lines in the reciprocal space were calculated with the LATLINE program (Agard, 1983).

Docking Procedures
The atomic model of the soluble StnII was visually fitted into the EM density envelope. Rebuilding to generate a model of a lipid-bound state was done using O (Jones et al., 1991). The final structure was energy minimized using the CNS software (Brünger et al., 1998). The fitting of the final high-resolution model of the lipid-bound state was further checked by docking it into the EM map with SITUS 2.1 (Chacón and Wriggers, 2002).

References

Agard, D.A. (1983). A least-square method for determining structure factors in three-dimensional tilted-view reconstructions. J. Mol. Biol. *167*, 849–852.

Amos, L.A., Henderson, R., and Unwin, P.N.T. (1982). Three-dimensional structure determination by electron microscopy of two-dimensional crystals. Prog. Biophys. Mol. Biol. *39*, 183–231.

Anderluh, G., and Macek, P. (2000). Cytolytic peptide and protein

toxins from the sea anemones (Anthozoa: Actiniaria). Toxicon *40*, 111–124.

Anderluh, G., Pungercar, J., Krizaj, I., Strukelj, B., Gubensek, F., and Macek, P. (1997). N-terminal truncation mutagenesis of equinatoxin II, a pore-forming protein from the sea anemone *Actinia equina*. Protein Eng. *10*, 751–755.

Anderluh, G., Barlic, A., Podlesek, Z., Macek, P., Pungercar, J., Gubensek, F., Zecchini, M.L., Serra, M.D., and Menestrina, G. (1999). Cysteine-scanning mutagenesis of an eukariotic pore-forming toxin from sea anemone: topology in lipid membranes. Eur. J. Biochem. *263*, 128–136.

Anderluh, G., Barlic, A., Potrich, C., Macek, P., and Menestrina, G. (2000). Lysine 77 is a key residue in aggregation of equinatoxin II, a pore-forming toxin from sea anemone *Actinia equina*. J. Membr. Biol. *173*, 47–55.

Athanasiadis, A., Anderluh, G., Macek, P., and Turk, D. (2001). Crystal structure of the soluble form of Equinatoxin II, a pore-forming toxin from the sea anemone *Actinia equina*. Structure *9*, 341–346.

Barton, G.J. (1993). ALSCRIPT: a tool for format multiple sequence alignments. Protein Eng. *6*, 37–40.

Bellamy, H.D., Lim, L.W., Mathews, F.S., and Dunham, W.R. (1989). Studies of crystalline trimethylamine dehydrogenase in three oxidation states and in the presence of substrate and inhibitor. J. Biol. Chem. *264*, 11887–11892.

Belmonte, G., Menestrina, G., Pederzolli, C., Krizaj, I., Gubensek, F., Turk, T., and Macek, P. (1994). Primary and secondary structure of a pore-forming toxin from the sea anemone, *Actinia equina* L., and its association with lipid vesicles. Biochim. Biophys. Acta *1192*, 197–204.

Berheimer, A.W., and Avigad, L.S. (1976). Properties of a toxin from the sea anemone *Stoichactis helianthus*, including specific binding to sphingomyelin. Proc. Natl. Acad. Sci. USA *73*, 467–471.

Billington, S.J., Jost, B.H., and Songer, J.G. (2000). Thiol-activated cytolysins: structure, function and role in pathogenesis. FEMS Microbiol. Lett. *182*, 197–205.

Brünger, A.T., Adams, P.D., Clore, G.M., DeLano, W.L., Gros, P., Grosse-Kunstleve, R.W., Jiang, J.S., Kuszewski, J., Nilges, M., Pannu, N.S., et al. (1998). Crystallography, and NMR system: a new software suite for macromolecular structure determination. Acta Crystallogr. D *54*, 905–921.

CCP4 (Collaborative Computational Project Number 4) (1994). CCP4 suite: programs for crystallography. Acta Crystallogr. D *50*, 760–763.

Chacón, P., and Wriggers, W. (2002). Multi-resolution contour based fitting of macromolecular structures. J. Mol. Biol. *317*, 375–384.

Crowther, R.A., Henderson, R., and Smith, J.M. (1996). MRC image processing programs. J. Struct. Biol. *116*, 9–16.

De los Ríos, V., Mancheño, J.M., Lanio, M.E., Oñaderra, M., and Gavilanes, J.G. (1998). Mechanism of the leakage induced on lipid model membranes by the hemolytic protein sticholysin II from the sea anemone *Stichodactyla helianthus*. Eur. J. Biochem. *252*, 284–289.

De los Ríos, V., Mancheño, J.M., Martínez del Pozo, A., Alfonso, C, Rivas, G., Oñaderra, M., and Gavilanes, J.G. (1999a). Sticholysin II, a cytolysin from the sea anemone *Stichodactyla helianthus,* is a monomer-tetramer associating protein. FEBS Lett. *455,* 27–30.

De los Ríos, V., Oñaderra, M., Martínez-Ruíz, A., Lacadena, J., Mancheño, J.M., Martínez del Pozo, A., and Gavilanes, J.G. (1999b). Overproduction in *Escherichia coli* and purification of the hemolytic protein sticholysin II from the sea anemone *Stichodactyla helianthus*. Protein Express. Purif. *18,* 71–76.

Esnouf, R.M. (1997). An extensively modified version of MolScript that includes greatly enhanced coloring capabilities. J. Mol. Graph. *15*, 132–134.

Gallivan, J.P., and Dougherty, D.A. (1999). Cation-π interactions in structural biology. Proc. Natl. Acad. Sci. USA *96*, 9459–9464.

Hardt, S., Wang, B., and Schmid, M.F. (1996). A brief description of I.C.E.: the integrated crystallographic environment. J. Struct. Biol. *116*, 68–70.

Henderson, R., Baldwin, J.M., Downing, K.H., Lepault, J., and Zemlin, F. (1986). Structure of purple membrane from *Halobacterium halobium*: recording, measurement, and evaluation of electron micrographs at 3.5 Å resolution. Ultramicroscopy *19*, 147–178.

Heuck, A.P., Tweten, R., and Johnson, A.E. (2001). β-barrel pore-forming toxins: intriguing dimorphic proteins. Biochemistry *40*, 9065–9073.

Hinds, M.G., Zhang, W., Anderluh, G., Hansen, P.E., and Norton, R.S. (2002). Solution structure of the eukariotic pore-forming cytolysin equinatoxin II: implications for pore formation. J. Mol. Biol. *315*, 1219–1229.

Hong, Q., Gutierrez-Aguirre, I., Barlic, A., Malovrh, P., Kristan, K., Podlesek, Z., Macek, P., Turk, D., Gonzalez-Manas, J.M., Lakey, J.H., et al. (2002). Two-step membrane binding by Equinatoxin II, a pore-forming toxin from the sea anemone, involves an exposed aromatic cluster and a flexible helix. J. Biol. Chem. *277*, 41916–41924.

Hovmöller, S. (1992). CRISP: Crystallographic image processing on a personal computer. Ultramicroscopy *41*, 121–135.

Jones, T.A., Zou, J.Y., Cowan, S.W., and Kjeldgaard, M. (1991). Improved methods for building protein models in electron density maps and the location of errors in these models. Acta Crystallogr. A *47*, 110–119.

Kem, W.R. (1988). Sea anemone toxin: structure and action. In The Biology of Nematocysts, D.A. Hessinger and H.M. Lenhoff, eds. (San Diego: Academic Press), pp. 375–405.

Killian, J.A., and von Heijne, G. (2000). How proteins adapt to a membrane-water interface. Trends Biochem. Sci. *25*, 429–434.

Leslie, A. (1994). MOSFLM User Guide, MOSFLM Version 5.2. (Cambridge, UK: MRC Laboratory of Molecular Biology).

Macek, P., Zecchini, M., Pederzolli, C., Dalla-Serra, M., and Menestrina, G. (1995). Intrinsic tryptophan fluorescence of equinatoxin II, a pore-forming polypeptide from the sea anemone *Actinia equina* L., monitors its interaction with lipid membranes. Eur. J. Biochem. *234*, 329–335.

Malovrh, P., Viero, G., Dalla Serra, M., Podlesek, Z., Lakey, J.H., Macek, P., Menestrina, G., and Anderluh, G. (2003). A novel mechanism of pore-formation: membrane penetration by the N-terminal amphipathic region of Equinatoxin. J. Biol. Chem. *278*, 22678–22685.

Martín-Benito, J., Gavilanes, F., de los Ríos, V., Mancheño, J.M., Fernández, J.J., and Gavilanes, J.G. (2000). Two-dimensional crystallization on lipid monolayers and three-dimensional structure of sticholysin II, a cytolysin from the sea anemone *Stichodactyla helianthus*. Biophys. J. *78*, 3186–3194.

Merritt, E.A., and Murphy, M.E.P. (1994). Raster3D version 2. A program for photorealistic molecular graphics. Acta Crystallogr. D *50*, 869–873.

Michaels, D.W. (1979). Membrane damage by a toxin from the sea anemone *Stoichactis helianthus*. I. Formation of transmembrane channels in lipid bilayers. Biochim. Biophys. Acta *555*, 67–78.

Navaza, J. (1994). AMoRe: an automatic package for molecular replacement. Acta Crystallogr. A *50*, 157–163.

Nicholls, A., Sharp, K.A., and Honig, B. (1991). Protein folding and association: insights from the interfacial and thermodynamic properties of hydrocarbons. Proteins *11*, 281–296.

Olson, R., Nariya, H., Yokota, K., Kamio, Y., and Gouaux, E. (1999). Crystal structure of Staphylococcal LukF delineates conformational changes accompanying formation of a transmembrane channel. Nat. Struct. Biol. *6*, 134–140.

Parker, M.W., Buckley, J.T., Postma, J.P., Tucker, A.D., Leonard, K., Pattus, F., and Tsernoglou, D. (1994). Structure of the Aeromonas toxin proaerolysin in its water-soluble and membrane-channel states. Nature *367*, 292–295.

Roderick, S.L., Chan, W.W., Agate, D.S., Olsen, L.R., Vetting, M.W., Rajashankar, K.R., and Cohen, D.E. (2002). Structure of human phosphatidylcholine transfer protein in complex with its ligand. Nat. Struct. Biol. *9*, 507–511.

Saibil, H.R. (2000). Conformational changes studied by cryo-electron microscopy. Nat. Struct. Biol. *7*, 711–714.

Saier, M.H., Jr. (2000). A functional-phylogenetic classification system for transmembrane solute transporters. Microbiol. Mol. Biol. Rev. *64*, 354–411.

Shaw, P.J., and Hills, G.J. (1981). Tilt specimen in the electron microscope: a simple specimen holder and the calculation of tilt angles for crystalline specimens. Micron *12*, 279–282.

Song, L., Hobaugh, M.R., Shustak, C., Cheley, S., Bayley, H., and Gouaux, J.E. (1996). Structure of staphylococcal alpha-hemolysin, a heptameric transmembrane pore. Science *274*, 1859–1866.

Stroud, R.M., Reiling, K., Wiener, M., and Freymann, D. (1998). Ion-channel-forming colicins. Curr. Opin. Struct. Biol. *8*, 525–533.

Sussman, J.L., Harel, M., Frolow, F., Oefner, C., Goldman, A., Toker, L., and Silman, I. (1991). Atomic structure of acetylcholinesterase from *Torpedo californica*: a prototypic acetylcholine-binding protein. Science *253*, 872–879.

Thomson, J.D., Gibson, T.J., Plewinak, F., Jeanmougin, F., and Higgins, D.G. (1997). The CLUSTALX window interface: flexible strategies for sequence alignment aided by quality analysis tools. Nucleic Acids Res. *24*, 4876–4882.

Valcárcel, C.A., Dalla Serra, M., Potrich, C., Bernhart, I., Tejuca, M., Martinez, D., Pazos, F., Lanio, M.E., and Menestrina, G. (2001). Effects of lipid composition on membrane permeabilization by Sticholysin I and II, two cytolysins from the sea anemone *Stichodactyla helianthus*. Biophys. J. *80*, 2761–2774.

Valpuesta, J.M., Carrascosa, J.L., and Henderson, R. (1994). Analysis of electron microscopy images and electron diffraction patterns of thin crystals of ϕ29 connectors in ice. J. Mol. Biol. *240*, 281–287.

Varanda, A., and Finkelstein, A. (1980). Ion and non electrolyte permeability properties of channels formed in planar lipid bilayer membranes by the cytolytic toxin from the sea anemone *Stoichactis helianthus*. J. Membr. Biol. *55*, 203–211.

Wimley, W.C., and White, S.H. (1996). Experimentally determined hydrophobicity scale for proteins at membrane interfaces. Nat. Struct. Biol. *3*, 842–848.

Yang, L., Harroun, T.A., Weiss, T.M., Ding, L., and Huang, H.W. (2002). Supramolecular structures of peptide assemblies in membranes by neutron off-plane scattering: method of analysis. Biophys. J. *81*, 1475–1485.

Accession Numbers

Coordinates have been deposited in the Protein Data Bank (accession codes 1GWY for StnII from type I crystals, 1O71 for the model of StnII from type II crystals, and 1O72 for the StnII:POC complex).